THE JOURNAL OF PHYSICAL CHEMISTRY B

Article

pubs.acs.org/JPCB

# Modulation of a Small Two-Domain Lipid Vesicle by Linactants

Zhenlong Li and Alemayehu A. Gorfe*

Department of Integrative Biology and Pharmacology, The University of Texas Medical School at Houston, 6431 Fannin Street, Houston, Texas 77030, United States

**ABSTRACT:** Linactants, molecules that preferentially localize at the boundary of lipid membrane domains, are attracting considerable attention in recent years due to the recognition that they might regulate lipid-phase separation and thereby modulate membrane morphology. Recent studies have also shown that clustering of some line active agents enhances their ability to modulate membrane curvature. However, the molecular origin of this phenomenon, and the degree to which it impacts biological membranes, remains poorly understood. In this work, we have investigated how linactants induce shape change in multidomain small unilamallar vesicles (SUVs) using extensive dissipative particle dynamics simulations. The linactant was modeled as a two-tailed hybrid lipid with the two tails differing in preference for different lipid domains. We found that addition of a small amount of linactants (~1%) to a two-domain vesicle leads to substantial reduction in the line tension and neck curvature at the domain boundary. Using cross-linking as a surrogate for clustering, we further show that linactant clusters substantially enhance the boundary preference and therefore the reduction in neck curvature. Moreover, on the basis of analyses of the corresponding changes in the membrane energetics, we highlight how linactants might stabilize nanoscale domains. These results have important implications for the potential existence and physical explanations of nanosized domains in biological membranes.

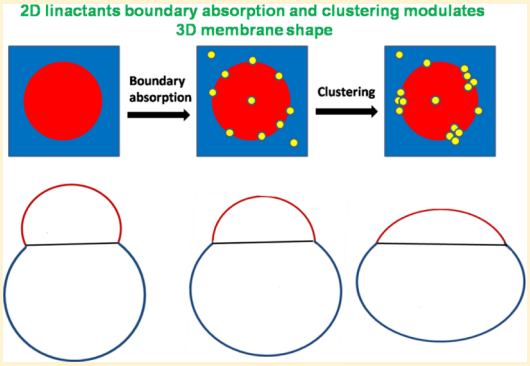


## INTRODUCTION

Deciphering the molecular mechanism by which the shape of a lipid bilayer membrane is modulated by changes in its composition is a fundamental challenge in membrane biophysics.[1,2] The challenge is particularly acute for multiphase bilayers in which the overall shape is a function of the composition and elastic property of multiple bulk domains as well as the boundary between them. For instance, the shape of a phase-separated lipid bilayer vesicle has been shown to depend on both the material property of the two bulk domains and the domain boundary.[2−5] It is therefore obvious that molecules that influence boundary properties can alter membrane shape. The goal of this work was to examine how linactants,[6] the 2D analog of surfactants, might modulate the shape of a two-domain vesicle.

Hybrid lipids, lipids made up of one saturated and one unsaturated fatty acyl chains, such as 1-palmitoyl-2-oleoylphosphatidylcholine (POPC), have received considerable attention as models of linactants.[7,8] For instance, using mean field theory, Safran et al.[7,9−11] predicted that hybrid lipids preferentially bind to the interface between liquid-ordered ($L_o$) and liquid-disordered ($L_d$) domains, which causes reduction of the boundary line tension and stabilization of finite-sized domains. Coarse-grained molecular dynamics (CGMD) simulations led to the same conclusion.[12] The resulting implication for the potential existence of nanoscale membrane rafts in living cells[13,14] inspired experimental biophysicists to use hybrid lipids as modulators of ternary lipid mixtures, typically comprising saturated and unsaturated lipids plus cholesterol.[15−19] It has been shown that POPC alters the phase diagram of a dipalmitoylphosphatidylcholine (DPPC), 1,2-dioleoyl-*sn*-glycero-3-phosphocholine (DOPC), and cholesterol mixture and transforms the macroscopic membrane domains into nanosized substructures.[15] Similarly, both experiments[20,21] and simulations[22−25] have shown that peptides containing palmitoyl plus farnesyl modifications segregate to the $L_o/L_d$ boundary. Aggregation enhances the boundary preference of these peptides,[22,23] possibly due to additive effects.[26,27] Moreover, Dinsmore and colleagues have shown that clustering of Ni-chelated lipids upon protein binding alters the shape of a phase-separated vesicle;[28] they rationalized this observation based on the idea that cluster-induced segregation of lipids to the domain boundary reduces line tension.

Because of resolution limits, it is difficult to experimentally characterize the effect of clustered linactants on membrane shape at the molecular level. As a result, there are very few studies that have tackled the issue directly. To examine the interplay between membrane curvature and aggregation of linactants in detail, here we used dissipative particle dynamics (DPD) simulations to investigate the shape change of a two-domain small unilamellar vesicle (SUV) upon the addition of small amounts of monomeric or cross-linked (dimer and pentamer) linactants. We discuss the changes in the shape and elastic energy of the vesicles induced by the linactants.

**Received:** April 30, 2014
**Revised:** July 7, 2014
**Published:** July 8, 2014

   dx.doi.org/10.1021/jp5042525 | *J. Phys. Chem. B* 2014, 118, 9028−9036

## METHODS

**Dissipative Particle Dynamics.** DPD is a particle-based simulation approach that uses simplified representation of a system and evolves interacting beads via Newtonian mechanics.[29−31] It is a mesoscopic method widely used to study pure and multicomponent lipid membranes.[32−38] The theoretical basis of the method was described in the original publication[31] as well as in our previous publication.[39] In brief, the pairwise nonbonded force $f_{ij}$ between beads $i$ and $j$ is represented by the summation of the conservative force ($f_{ij}^{C}$), the random force ($f_{ij}^{R}$), and the dissipative force ($f_{ij}^{D}$)

$$f_{ij} = f_{ij}^{C} + f_{ij}^{D} + f_{ij}^{R} \quad (1)$$

All three forces share the same cutoff distance $r_c = d_0$, which becomes zero when $r_{ij} > r_c$. Within the cutoff distance

$$f_{ij}^{C} = a_{ij}\left(1 - \frac{r_{ij}}{r_c}\right)\hat{r}_{ij} \quad (2)$$

$$f_{ij}^{D} = -\gamma\omega^{D}(r_{ij})(\hat{r}_{ij}\cdot\hat{v}_{ij})\hat{r}_{ij} \quad (3)$$

$$f_{ij}^{R} = \sigma\zeta_{ij}\omega^{R}(r_{ij})\hat{r}_{ij} \quad (4)$$

where $a_{ij}$ is the repulsive interaction parameter between $i$ and $j$, $r_{ij} = |r_i - r_j|$, and $v_{ij} = |v_i - v_j|$. $\gamma = 3.0k_bT/d_0^2$ is the friction coefficient and $\sigma$ is the noise amplitude that satisfies $\sigma^2 = 2\gamma k_bT$.[31] $w^D$ and $w^R$ are the weight functions with $w^D = (w^R)^2 = (1 - r_{ij}/r_c)^2$. $\zeta_{ij}$ is a Gaussian random number. Throughout this article, we use reduced DPD units where mass and length are described in units of particle mass ($m_0$) and diameter ($d_0$) that are taken to be unity, respectively.

**Model Systems.** Our coarse-grained model systems comprised three types of lipid (lipid A, lipid B, and hybrid lipid AB) plus water (W). The three lipids shared the same amphiphilic architecture $H_4(T_4)_2$, where H represents the hydrophilic headgroup and T is hydrophobic tail. The only difference among them was in the nonbonded conservative interaction parameter at the tail region (Figure 1 and Table 1); this difference induces immiscibility (see later). Whereas water molecules were modeled by single beads, adjacent beads in lipids were connected by a harmonic potential $E_{bond} = 1/2k_{bond}(r_{ij} - b_0)^2$ (Figure 1), where $r_{ij}$ is the distance between two connected beads. We used a force constant $k_{bond} = 100k_bT/d_0^2$ and equilibrium bond length $b_0 = d_0$ for all bonds except that between bead 3 and 4, for which a shorter bond length $b_0 = 0.8d_0$ was used (Figure 1). Lipid tail chain rigidity was maintained by applying a harmonic angle potential $E_{angle} = 1/2k_{angle}(\theta - \theta_0)^2$ with $k_{angle} = 50k_bT$ to all angles $\theta$ except the angle subtended by beads 1, 2, and 4. The equilibrium angle $\theta_0$ was set to 120° for the angle between beads 2, 3 and 4, and 180° for all others. This lipid topology is to some extent similar to the DPPC model in the coarse-grained Martini biomolecular force field,[40] in which on average four heavy atoms are mapped into one bead.

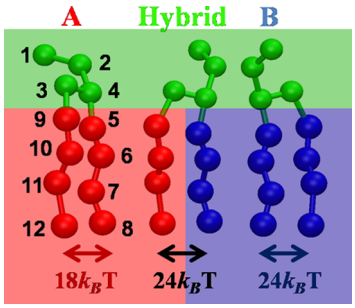


**Figure 1.** Lipid models and DPD conservative interaction parameters. Lipid A (left), lipid B (right), and hybrid lipid (middle) all have same architecture $H_4(T_4)_2$ and same labeling of beads, as shown for lipid A. They also have the same hydrophilic headgroup bead type H (green). The hydrophobic tail beads of lipid A ($T_A$) and B ($T_B$) are in red and blue, respectively. The intra- and intermolecular interaction parameters between lipid type A tail beads, lipid B tail beads, and hybrid lipid tail beads are also highlighted. For clarity, in subsequent figures, lipids A and B and the hybrid lipid will be represented in red, blue, and light green, respectively.

**Table 1. Conservative Interaction Parameters for Lipids and Water Used in Our DPD Simulations[a]**

| | $H$ | $T_A$ | $T_B$ | $W$ |
|---|---|---|---|---|
| $H$ | 40 | 50 | 50 | 35 |
| $T_A$ | | 18 | 24 | 75 |
| $T_B$ | | | 24 | 75 |
| $W$ | | | | 25 |

[a] $H$: headgroup, $T_A$: tail of lipid A, $T_B$: tail of lipid B, and $W$: water. Unit: $k_bT/d_0$.

**Parameterization.** Previous studies have used various strategies to induce phase separation during DPD simulation of multicomponent lipid bilayers.[33,37] We adopted the one by Illya et al. in which phase separation between two types of lipids was dictated by the repulsion at the tail region.[33] Because lipid types A and B in our model differ only in their tail (Table 1), the repulsive parameters were set to be $18k_bT/d_0$ for $T_A$ ($a_{TAA}$) and $24k_bT/d_0$ for $T_B$ ($a_{TBB}$) and the cross-interaction between $T_A$ and $T_B$ ($a_{TAB}$). This allows for type A lipids to form a more packed bilayer (smaller $a_{TAA}$) than type B lipids; when mixed, the two lipids would form a raft-like and a more dynamic non-raft-like domain, respectively. While sharing the same H with both lipids A and B, one tail of the hybrid lipid is type $T_A$, while the other is $T_B$ (Figure 1), so that it has no clear preference for either type of the nonhybrid lipids. Finally, the repulsive interaction parameter between the water beads ($a_{WW}$) was set to $25k_bT/d_0$. The average number density of beads in the simulation box was set to three and maintained by periodic boundary condition. This setup reproduces the compressibility of water at room temperature.[31] Additional details are listed in Table 1.

**System Setup and Simulation Protocol.** An initial bilayer was built from 1536 type A lipids randomly dispersed in a water box of $30d_0 \times 30d_0 \times 30d_0$, which quickly self-assembled into a planar bilayer when simulated at constant volume and temperature (NVT ensemble, see later). Starting from this bilayer, planar and vesicular bilayer systems of various size and composition (containing either lipid type A, type B, or mixtures thereof) were constructed and simulated, as follows.

*i. Pure Planar Bilayers.* First, we built bilayers made up of 288 type A or type B lipids per leaflet and simulated them under the condition of constant surface area (fixing the $x$ and $y$ dimensions of the simulation box) to study the structure and mechanical properties of bulk domains. In these simulations, each bilayer was first simulated at $P = 23.9k_bT/d_0^3$ and $k_bT = 1$ for 100 000 steps to allow the bilayer to adjust freely to a nearly tensionless state, followed by 1 000 000 time steps of NVT run at the same temperature. The resulting system was used to


dx.doi.org/10.1021/jp5042525 | J. Phys. Chem. B 2014, 118, 9028−9036

begin multiple NVT simulations for the same duration (1 000 000 time steps) after introducing small tensions by increasing the surface area of the simulation box by 1, 2, 3, and 4%. In each case, coordinates and pressure tensors were recorded every 100 time steps for the calculation of bilayer thickness and surface tension.

*ii. Two-Domain Planar Bilayers with and without Hybrid Lipids.* The following were used to study the influence of hybrid lipids on a two-main bilayer. First, we built a two-domain bilayer by merging bilayers of pure lipids A and B (each containing 576 lipids per leaflet). Then, we duplicated the system and added 0, 100, 200, and 300 hybrid lipids evenly distributed on both leaflets. The systems were equilibrated and simulated for 20 000 000 steps under the NVT ensemble ($k_bT$ = 1). Coordinate positions and pressure tensors of the simulation box were recorded every 1000 steps for the analysis of lipid distribution and line tension.

*iii. Two-Domain Vesicles without Hybrid Lipids.* We prepared a bilayer vesicle through the bilayer-to-vesicle transition process of a large planar bilayer.[41] A large bilayer of 9216 lipids was prepared by duplicating (in a 3 × 3 grid) a symmetric planar bilayer containing 1024 randomly dispersed A- and B-type lipids (1:1 ratio). The resulting bilayer was placed at the center of a $80d_0 \times 80d_0 \times 60d_0$ water box, equilibrated, and simulated under NVT for 10 000 steps using the same repulsive parameter for all lipid tails ($a_{TAA} = a_{TBB} = a_{TAB} = 20k_bT/d_0$). Then, the respective repulsive parameters of A and B lipids were applied to allow for phase separation and vesicle closure during an extended simulation of up to 50 000 000 steps, which was used to study the equilibrium shape of the vesicles.

*iv. Two-Domain Vesicles with Hybrid Lipids.* To simulate a two-domain vesicle containing monomeric hybrid lipids, we conducted simulations of the bilayer-to-vesicle transition for the same large planar bilayer previously described but after hybrid lipids were randomly inserted into the two leaflets (before the bilayer was put into the water box). To simulate a two-domain vesicle with clustered hybrid lipids, we cross-linked the hybrid lipids using a harmonic potential $E_{bond} = 1/2k_{bond}(r_{ij} - b_0)^2$ with $k_{bond} = 100k_bT/d_0^2$ and $b_0 = d_0$. Specifically, dimers and pentamers were made by linear cross-linking of every two and five neighboring hybrid lipids at the headgroups. Each system was then re-equilibrated and simulated as described in section iii, recording coordinates every 1000 steps for data analysis.

All of the simulations were conducted with the open-source molecular dynamics simulation package LAMMPS[42] using an integration time step of $0.02(m_0d_0^2/k_bT)^{1/2}$.

**Vesicle Shape Analysis.** Analysis of the well-equilibrated portion of the vesicle simulations indicated that the final shape of the vesicle was axis-symmetric, with the two domains sharing a joint principal axis. Each vesicle was therefore divided into three parts along the principal axis, yielding two hemispherical rims connected by a cylindrical barrel. For comparison and quantitative analysis, a 2D contour line was constructed for each vesicle using the position of the lipid tail end beads. To achieve this, at each saved time step the geometric center of the vesicle was first shifted to the origin and then aligned along the $z$ axis using the joint principal axis, with domain A placed to the left side (Figure 2). The distance of each tail end bead to the $z$ axis ($r$) and its $z$ position ($z$) was projected to a $z$−$r$ plane as point ($z$, $r$). The contour of the vesicle was then constructed using this 2D representation based on the following procedure. First, the 2D projection was divided into equal bins of size $0.2d_0$ along $z$, and the average $r$ was calculated for each bin and plotted against the $z$ positions. To determine the two barrel-rim boundaries, the curve was divided into two parts at the origin. For each part, the rim-barrel boundary was determined as the $z$ position where the average $r$ is the maximum. The curve between the two boundaries thus represents the contour of the barrel. To calculate the contours of the two rims, we used each $z$ position on the $z$ axis of a barrel-rim boundary as a center to divide all points on the rim into equal angular bins of size 1°. For each bin, the average position of all points was calculated and plotted as the 2D contour of the rim. The 2D contours of the two rims and the barrel match seamlessly at the rim-barrel boundaries. The boundary of the two domains was determined as the $z$ position where the mole fraction of lipids A and B is equal.

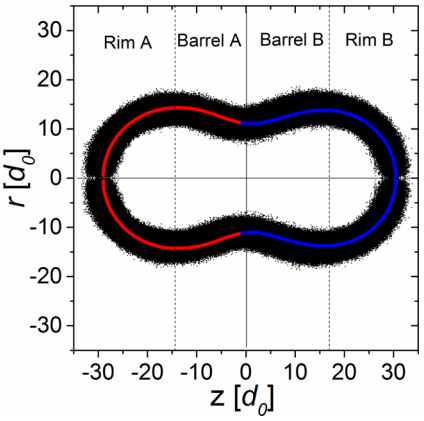


**Figure 2.** Construction of a 2D contour line to show the average shape of vesicles derived from DPD simulation trajectories. The vertical dashed lines indicate the boundaries between the barrel and the rims.

## RESULTS AND DISCUSSION

The current work was motivated by our previous CGMD studies of surface-bound lipid-modified Ras peptides containing two saturated palmitoyl and one unsaturated farnesyl lipid, where we observed that partitioning of the clustered fraction of the peptides into the domain boundary reduces the line tension and modulates curvature.[22,23] However, because the self-assembled clusters were polydisperse in size in both the previous CGMD[22,23] and new DPD simulations (not shown), it was difficult to unambiguously quantify the relationship between cluster size and line tension. We therefore focused on cross-linked hybrid lipids of predetermined sizes as surrogates for finite-sized, self-assembled linactive peptides to directly quantitate the effect of cluster size on membrane curvature.

**Linactants Modulate Membrane Domain Boundary Line Tension.** Numerous studies have shown that line tension is an important parameter controlling the shape of multidomain membranes.[2,3,5,28,43−45] For example, using continuum elasticity theory, Lipowsky and colleagues have shown that the total free energy of a two-domain bilayer can be described as the sum of the domain bending and boundary line energies and predicted line tension-induced shape transition for both planar bilayers and vesicles.[5,43] Baumgart et al. visualized the shape of multidomain vesicles using two-photon microscopy and quantified the relation between vesicle shape and membrane mechanical properties, including elasticity moduli and line tension.[3,45] Taken together, these studies indicate that


dx.doi.org/10.1021/jp5042525 | J. Phys. Chem. B 2014, 118, 9028−9036

partitioning and self-aggregation of linactants at the domain boundary can potentially affect membrane shape by modifying the line tension.

To quantify the effect of boundary-bound linactacts on the line tension of our model membranes, we first need to estimate the average area per lipid $A_{pr}$ and surface tension $\gamma$ of the bilayers of pure lipid type A and type B simulated at different surface area conditions. $A_{pr}$ was estimated simply from the area of the simulation box ($L_x \times L_y$) divided by the number of lipids per monolayer ($N_l$), where $L$ is lateral dimension of the box along the $x$ and $y$ dimension and $N_l$ is one-half of the total number of lipids. $\gamma$ was calculated as[46]

$$\gamma = \frac{L_z}{2}\left\langle P_{zz} - \frac{1}{2}(P_{xx} + P_{yy})\right\rangle \quad (5)$$

where $L_z$ is the simulation box length in the $z$ dimension and $P_{xx}$, $P_{yy}$, and $P_{zz}$ are the pressure tensors. Standard deviations were calculated by block-averaging of the pressure tensors.[47] Plots of $\gamma$ versus $A_{pr}$ (Figure 3) show a linear relation for both

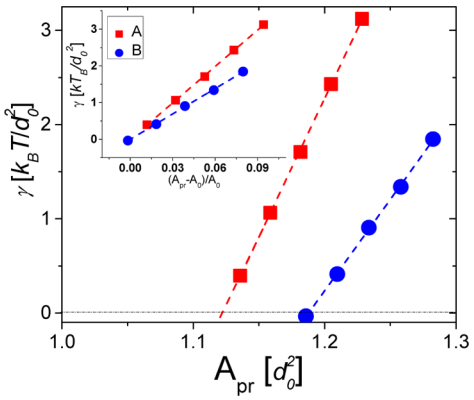


**Figure 3.** Bilayer surface tension ($\gamma$) versus area per lipid ($A_{pr}$) derived from simulations of bilayers made up of lipid type A (red) or B (blue). Inset: $\gamma$ versus normalized area expansion ($(A_{pr} - A_0)/A_0$), where $A_0$ is the average tensionless area per lipid obtained from extrapolation of the curves in the main plot to $\gamma = 0$ (dotted horizontal line).

bilayers A and B, which is expected because the simulations were at small tension regimes.[46] By extrapolating the linear fit to $\gamma = 0$, we obtained the tensionless average area per lipid $A_0$ for each type of lipid (Table 2).

**Table 2. Summary of Bilayer Structural and Mechanical Properties**[a]

| bilayer | A | B |
|---|---|---|
| $A_0$ [$d_0^2$] | 1.12 ± 0.01 | 1.19 ± 0.02 |
| $h_{bi}$ [$d_0$] | 6.6 ± 0.1 | 6.6 ± 0.1 |
| $K$ [$k_bT/d_0^2$] | 33.0 ± 0.2 | 23.0 ± 0.2 |
| $\kappa_b$ [$k_bT$] | 29.9 ± 0.2 | 20.9 ± 0.2 |

[a] $A_0$: area per lipid, $h_{bi}$: bilayer thickness, $K$: area stretching modulus, and $\kappa_b$: bending modulus.

Once we have $A_{pr}$ and $A_0$, the bilayer area-stretching modulus $K$ can be estimated from a linear fit of the $\gamma$ (eq 5) versus $(A_{pr} - A_0)/A_0$ curve (Figure 3 inset)[46]

$$\gamma \approx K(A_{pr} - A_0)/A_0 \quad (6)$$

The bilayer bending modulus $\kappa_b$ can then calculated from the relation[48]

$$\kappa_b = Kh_{bi}^2/48 \quad (7)$$

where $h_{bi}$ is the tensionless bilayer thickness defined as the average head-to-head distance between the two leaflets. The results of these analyses are listed in Table 2 for both pure bilayers A and B. As expected from our parametrization (i.e., the repulsion among the tails of the A lipids is smaller than that of the B lipids), bilayer A is more tightly packed with smaller area per lipid and has larger area stretching and bending moduli.

For bilayers containing two stripped domains, the domain boundary was found to be a ~5$d_0$-wide interface characterized by a sharp transition in lipid composition (Figure 4a). The

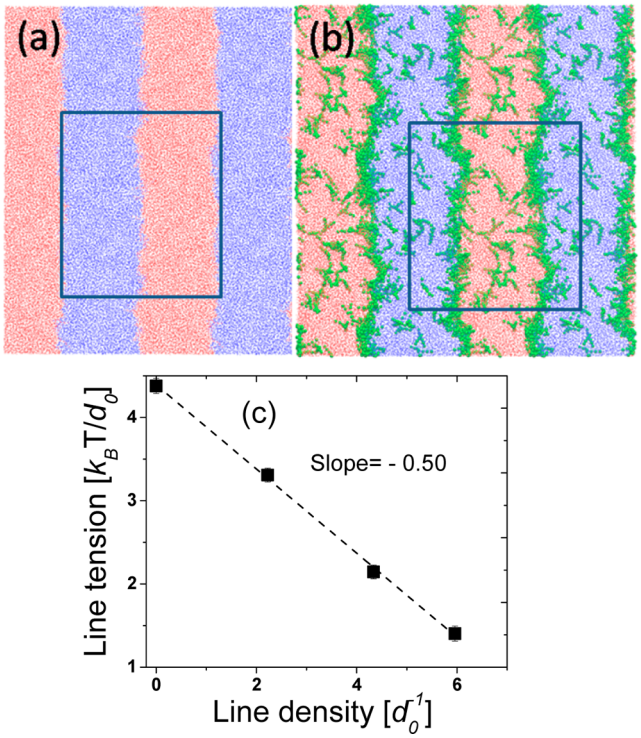


**Figure 4.** Lateral distribution and effect of linactants on a two-domain bilayer. (a) Final snapshot of a reference two-domain bilayer without hybrid lipids. (b) Final snapshot of a two-domain bilayer containing 100 monomeric linactants. In each case, the blue line represents the actual simulation box. Red dots represent lipid A and blue dots lipid B, while green spheres represent the hybrid lipid. (c) Line tension of a two-domain bilayer as a function of the number of linactants per unit length (line number density) of the domain boundary.

boundary line tension $\sigma$ was estimated from the pressure tensors (eq 8)[49]

$$\sigma = \frac{1}{2}\langle L_xL_z(P_{xx} - P_{yy})\rangle \quad (8)$$

where $L_x$ and $L_z$ are the simulation box lengths along the $x$ and $z$ dimensions, respectively, and $P_{xx}$ and $P_{yy}$ are the respective pressure tensors perpendicular and parallel to the domain boundary along the $x$ dimension. $\sigma$ was estimated to be 4.38 ± 0.08$k_bT/d_0$ for the linactant-free bilayer (Figure 4c), which is sufficiently large to induce lipid-phase separation and maintain a fluctuating boundary. The addition of hybrid lipids did not affect the phase separation behavior, but their accumulation at the boundary appears to increase the extent of the boundary fluctuation (Figure 4b). To estimate the efficacy of the


dx.doi.org/10.1021/jp5042525 | J. Phys. Chem. B 2014, 118, 9028−9036

linactants to reduce line tension, we calculated $\sigma$ and the line number density of linactants at the domain boundary assuming uniform distribution (i.e., number of linactants at the boundary per unit length). This was done for bilayers containing the same number of A- and B-type lipids but different total number of linactants (0, 100, 200, 300). The plot in Figure 4c shows that $\sigma$ is correlated linearly with the number density, indicating that in all simulations the linactant concentration was small and does not saturate the boundary region. The slope of a linear fit of this curve quantifies the reduction in line tension per linactant molecule, which is equal to $-0.50k_bT$. Clearly, accumulation of linactants at domain boundaries significantly reduces the line tension.

**Two-Domain Vesicle with Neck Curvature.** The stationary shape of the linactant-free two-domain vesicle is an axisymmetric dumbbell with the two domains separated by a curved neck (Figure 5a). Each domain contains two rims and a cylindrical barrel. Because of the elastic nature of lipid bilayers, the average shape of each rim resembles a hemisphere, with the radius of rim A ($r_A$ = 14.3 ± 0.1$d_0$) being slightly larger than rim B ($r_B$ = 13.8 ± 0.1$d_0$; see Table 3). The length of barrel B along the $z$ axis is larger than that of barrel A ($l_B$ = 17.8 ± 0.1$d_0$ vs $l_A$ = 13.8 ± 0.2$d_0$), reflecting the fact that lipid B has larger area per lipid than A. Notice that each barrel smoothly transitioned from the rims to the boundary to avoid a steep change in bilayer surface shape that could have led to exposure of the hydrophobic lipid tails to water. The fact that the domain boundary has the smallest radius ($r_{AB}$ = 11.2 ± 0.1$d_0$) suggests the induction of neck curvature, which arises from the competition between domain bending and boundary contraction.[43]

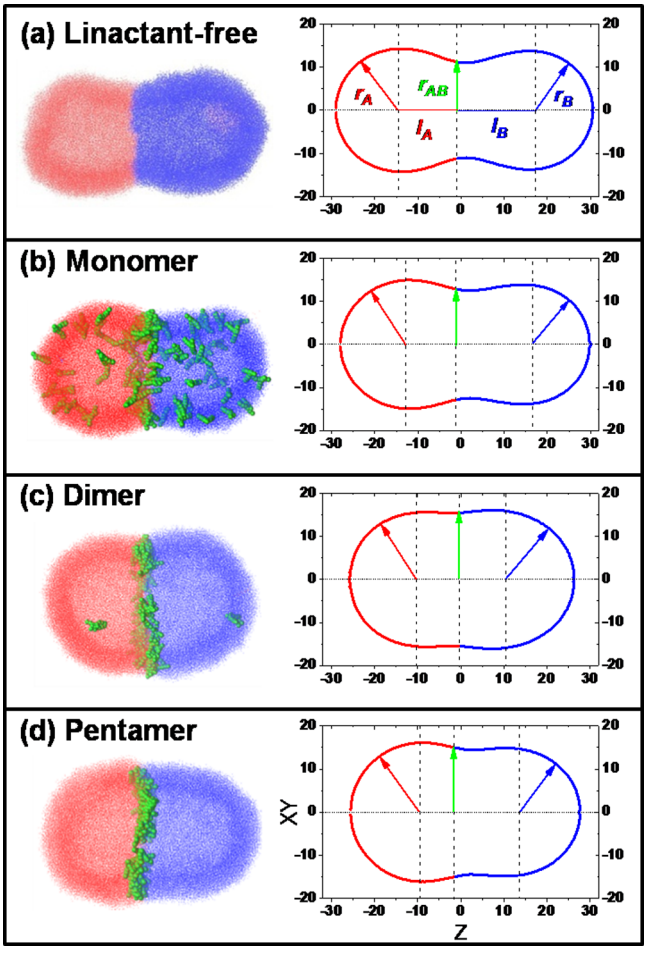


**Figure 5.** Snapshots (left) and 2D contour lines (right) of two-domain vesicles. (a) Vesicle without linactants. (b) Vesicle with 100 monomeric hybrid lipids. (c) Vesicle with 100 dimeric hybrid lipids. (d) Vesicle with 100 pentameric hybrid lipids. Color scheme for the snapshots: lipid A: red, lipid B: blue, and hybrid lipid: green.

**Table 3. Vesicle Size in Unit of $d_0$[a]**

| linactant | $r_A$ | $r_B$ | $r_{AB}$ | $l_A$ | $l_B$ |
|---|---|---|---|---|---|
| no | 14.3 | 13.8 | 11.2 | 13.8 | 17.8 |
| monomer | 15.0 | 13.8 | 12.9 | 11.8 | 17.2 |
| dimer | 15.6 | 15.9 | 15.5 | 10.6 | 11.4 |
| pentamer | 16.1 | 14.7 | 14.9 | 8.4 | 14.4 |

[a]Vesicle sizes were derived from the 2D contours shown in Figure 5. $r_A$: radius of rim A, $r_B$: radius of rim B, $r_{AB}$: radius of the domain boundary, $l_A$: length of barrel A, and $l_B$: length of barrel B. The standard deviations are 0.1 to 0.2$d_0$ for all.

The free energy of a two-domain membrane has contributions from the energy of bending of the two bulk domains and the line energy at the boundary.[5] The bending energy is proportional to domain curvature, whereas the line energy is proportional to the boundary length (and the line tension). Therefore, while resistance of the two domains to bending deformation tends to reduce expansion, the tendency of the domain boundary to minimize incompatible contacts would reduce the length of the boundary perimeter. The balance between the two thus determines the stationary shape of the vesicle. As a result, the critical length (concomitant length) for a domain to form a bud is determined by the ratio between the bending modulus of the center domain and the boundary line tension.[5] In our case, if we take domain A as the center domain and B as the surrounding domain, then the concomitant length becomes $\kappa_{b,A}/\sigma \approx 6.8d_0$, using $k_{b,A}$ = 29.9$k_bT$ (Table 1) and $\sigma$ = 4.38$k_bT/d_0$ from the previous section. The fact that this value is smaller than the minimum radius ($r_{AB}$ = 11.2 ± 0.1$d_0$) throughout the vesicle explains why we observed neck curvature in a small vesicle.

**Monomeric Linactants Reduce Neck Curvature in Bilayer Vesicles.** The addition of a small amount of linactants (100, < 1%) substantially altered the vesicle shape (compare Figure 5a,b; see Table 3). Although the overall shape of this vesicle resembles that of the linactant-free vesicle, the radii of rim A and the boundary are larger (by up to 16%). While the larger radius of rim A means that barrel A is less curved (shorter length along the $z$ axis), the diminution of the difference between the rim and boundary radii lowers the neck curvature (Figure 5a,b).

Visual inspection (Figure 5b) suggests that the linactacts are distributed primarily at the domain boundary but also across the two bulk domains. This is quantified in Figure 6a, which shows that on average ~44% (see Figure 6d) of the linactants are located at the boundary, defined as the region between $z$ = $-2d_0$ and $z$ = $4d_0$ based on the density profiles of lipids A and B. The question is what would be the impact of this boundary localization on the membrane elastic property and the reduced curvature at the boundary? Assuming that the efficiency of the hybrid lipids to reduce line tension is the same in planar bilayers and vesicles, one can estimate the overall reduction of the line tension ($\delta\sigma$) in the vesicle by the 44 (out of 100) monomeric hybrid lipids that localize at the domain boundary.


dx.doi.org/10.1021/jp5042525 | J. Phys. Chem. B 2014, 118, 9028−9036

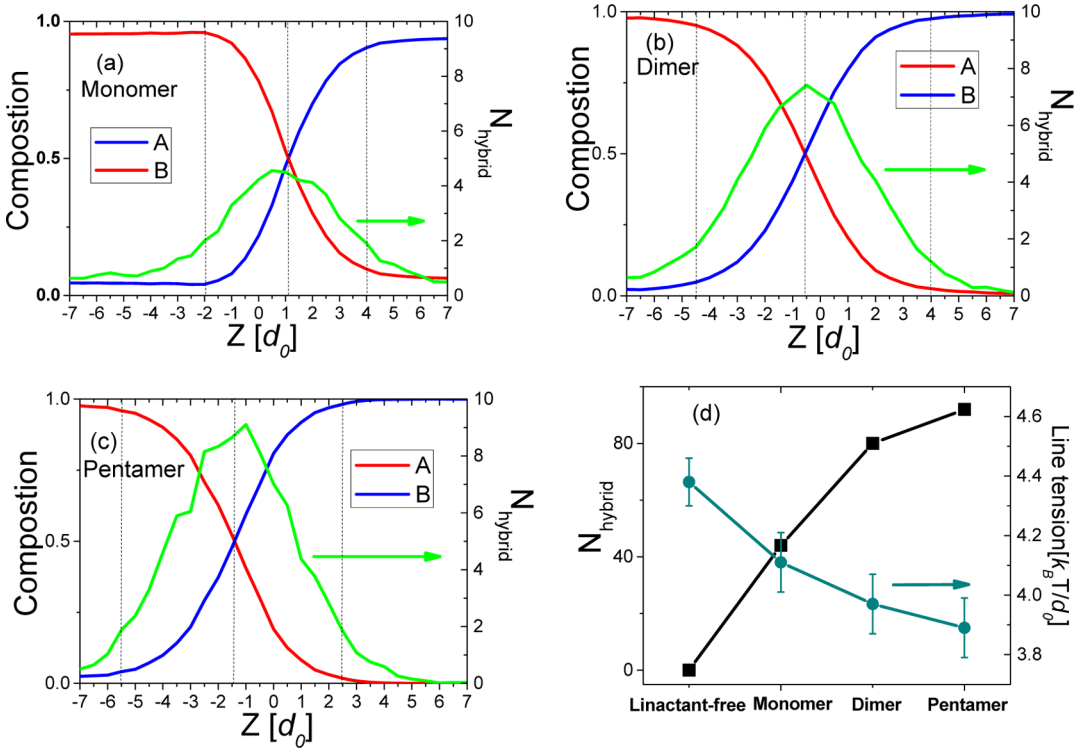


**Figure 6.** Distribution of lipids and linactants. (a) Lipid distribution profile in a vesicle with 100 monomeric hybrid lipids. (b) Lipid distribution profile in a vesicle with 100 dimeric hybrid lipids. (c) Lipid distribution profile in a vesicle with 100 pentameric hybrid lipids. (d) Number of hybrid lipids at the domain boundary and the estimated line tension for different vesicles. The density profiles of lipid A and B were normalized by the sum of the number of the two lipid types at each $z$ position. The absolute number of lipids was used for linactants.

For this, we used (i) the perimeter of the circular domain boundary, which is estimated from the radius to be 81.0 ± $0.1d_0$, and (ii) the linactant efficiency obtained from planar bilayers ($0.5k_bT$, section A). This yields $\delta\sigma \approx (44 \times 0.5)/81 = 0.27k_bT/d_0$. It is remarkable that such a small change in line tension could cause global change in the vesicle shape.

**Clustering of Linactants Enhances Domain Partitioning and Vesicle Shape Change.** In the presence of dimeric linactants, the vesicle adopted a nearly ellipsoid geometry with an almost flat barrel region (Figure 5c). Quantitatively, we find that the radii of the rims ($r_A$ = 15.6 ± $0.1d_0$ and $r_B$ = 15.9 ± $0.1d_0$, Table 3) and the barrel in the boundary ($r_{AB}$ = 15.5 ± $0.1d_0$) have become nearly identical and much larger than that of the linactant-free and monomer-bearing vesicles (Table 3). Concomitantly, $l_A$ and $l_B$ have decreased significantly (Table 3). This change of the vesicle shape is directly related to the dramatic increase in the number of cross-linked linactants at the boundary (Figures 5c and 6b); ~80 hybrid lipids have migrated to the boundary region ($z = -4.5$ to $z = 4.0d_0$). This represents an ~82% increase in boundary preference compared with the monomer, suggesting an additive behavior of linactant's domain preference (Figure 6b,d). Assuming that our surrogate for clustering (i.e., cross-linking) does not affect the property of linactants other than their domain preference, we estimate that $\delta\sigma \approx 0.41k_bT/d_0$.

To further test our hypothesis that enhanced clustering of linactants increases their boundary preference and thereby their effect on the line energy, we simulated a vesicle with the same total number (100) of linactacts but with every five molecules cross-linked. The number of pentameric linactants at the domain boundary has increased relative to dimers (Figure 6c,d), showing once again that clustering modulates domain preference. As in the dimers, pentamers reduced the overall curvature of the vesicle (Figure 5). However, a closer look at the radii of the rims and the boundary as well as the barrel lengths indicates that the effect of the pentameric linactants on the vesicle shape is nonuniform (Table 3). Notably, the pentamers have introduced significant asymmetry in curvature. (Notice that the neck curvature was slightly larger compared with the one with dimers.) We find $\delta\sigma \approx 0.49k_bT/d_0$ for the pentamers. Clearly, while our conclusion that clustering increases linactant efficiency remains unchanged, the fact that we find slightly larger curvature with the pentamers suggests that the exact size of the clusters is also important. We speculate that tighter arrangement of large aggregates undermines linactant efficiency, possibly because the larger clusters do not distribute uniformly throughout the domain boundary perimeter.

**Interplay between Domain Bending and Boundary Contraction.** In the previous sections, we have seen that as linactants migrate to the domain boundary the length of the boundary increases due to line tension reduction accompanied by an overall decrease in vesicle curvature. To evaluate, in an approximate fashion, the interplay between domain bending energy $E_b$ and line energy $E_l$, we turned to the theory of continuum membrane elasticity. According to this theory, $E_b$ can be estimated using the Helfrich curvature energy functional (eq 9)[50]

$$E_b = \int dA \, \frac{\kappa_b}{2}(C_1 + C_2)^2 \tag{9}$$

where $C_1$ and $C_2$ are the principal curvatures. Contribution from Gaussian curvature was not considered because the shape of all of our vesicles was similar.[43,50] For each domain, the


dx.doi.org/10.1021/jp5042525 | J. Phys. Chem. B 2014, 118, 9028−9036

geometric curvature of the rims and the barrel were calculated from their radii (Table 3), so that $E_b$ of the rim ($E_{b,rim}$) can be calculated as (eq 10)

$$E_{b,rim} = 2\pi r_{rim}^2 \frac{\kappa_b}{2}\left(\frac{1}{r_{rim}} + \frac{1}{r_{rim}}\right)^2 = 4\pi\kappa_b \quad (10)$$

where $r_{rim}$ is the rim radius. The bending energy of each barrel ($E_{b,cyl}$) was calculated by dividing it into $i$ small cylinders of length $dl = 0.2d_0$ along the $z$ direction (eq 11)

$$E_{b,cyl} = \sum_i 2\pi r_i dl \frac{\kappa_b}{2}\left(\frac{1}{r_i} + \frac{1}{\infty}\right)^2 = \pi dl\, \kappa_b \sum_i \frac{1}{r_i} \quad (11)$$

where $r_i$ is the average radius of each cylinder. The bending energies of all four parts were then combined to obtain the total bending energy. Finally, the line energy was calculated as the product of line tension (Figure 6d) and boundary length (Table 3).

As shown in Figure 7a, for each vesicle, $E_b$ is much larger than $E_l$ and decreases upon the addition of monomeric and multimeric linactants, as does the total free energy (sum of $E_b$ and $E_l$; see Figure 7b). Interestingly, although the line tension is reduced by linactants, the line energy actually increased due to the increase in the boundary length (Figure 7a). These results clearly illustrate that remodeling of membrane shape by linactants is a dynamic process governed by the global energy change.

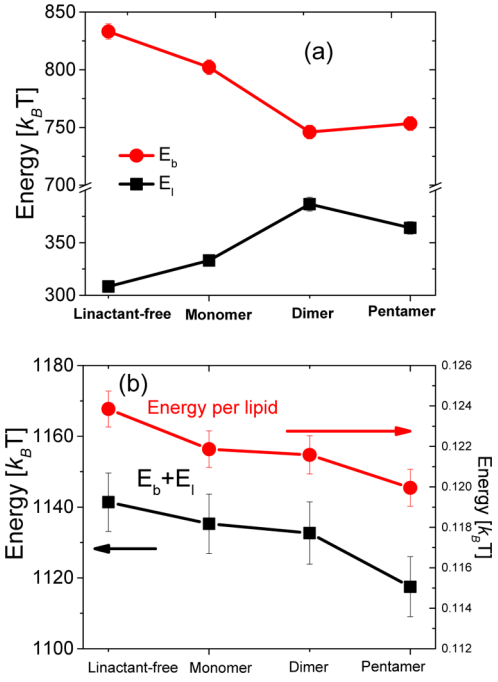


**Figure 7.** Effect of linactants on the energetics of vesicles. (a) Domain bending energy ($E_b$) and line energy ($E_l$) of vesicles without and with 100 monomeric, dimeric, and pentameric linactants. (b) $E_b + E_l$ before (black) and after (red) normalization by the total number of lipids in each vesicle to account for the different number of lipids in the simulations.

## CONCLUDING REMARKS

A number of membrane species that exist as monomers or oligomers have been identified as having preference for membrane domain boundaries.[14] The 2D microemusion effect of these linactants offers an appealing mechanism to explain the physical origin for the formation and stability of finite-sized membrane domains.

We studied the influence of linactant domain partitioning and self-aggregation on the shape of a two-domain vesicle. Whereas the effect of linactants on domain boundary fluctuation of planar membranes has been recently investigated using mean field theory and CGMD simulations,[8] our robust DPD simulations allowed us to investigate the issue in a closed membrane system. A two-domain vesicle is a common model to investigate the basic principles of membrane shape generation through domain-based lipid lateral organization. However, it remains a challenge to study vesicles using atomically detailed simulations. The DPD model used in our simulations represents a compromise between system resolution and computational efficiency. By omitting the chemical structure details, our model made it possible to simulate the formation and phase-separation processes of two-domain vesicles containing thousands of lipids. It is worth pointing out that the line tension effect on vesicle shape should only be observable when the line energy is of comparable magnitude to the domain binding energy. For example, for model membranes with coexisting $L_o$ and $L_d$ domains, the critical length for domain budding is relatively large and the line tension effect would be seen only in giant vesicles.[3,5] Additionally, the efficiency of linactants depends on their structure, as well as the structure of the domain boundary. In this work, the linactant was modeled as a hybrid lipid that was not parametrized to represent any specific hybrid lipid.

Using this approach, we found that domain contraction can induce neck curvature at the domain boundary of a linactant-free two-domain vesicle, which is consistent with previous experimental and theoretical studies.[3,5] The addition of monomeric linactants reduced the line tension, which led to relaxation of the domain boundary and therefore smaller neck curvature. Cross-linking of linactants as a surrogate for clustering enhanced the partitioning preference and further reduced or eliminated the neck curvature. By analyzing the vesicle shape and energetics, we were able to systematically quantify the influence of linactant partitioning and aggregation on vesicle shape. Our simulations not only suggest that the 2D segregation of linactants can influence the 3D shape of the host membrane but also allowed us to decipher the underlying mechanism, namely, clustering and boundary partitioning are directly coupled to reduction in line energy and hence membrane curvature. This mechanism has broad implications for membrane shape generation in cells because it provides a fresh perspective into how common hybrid lipids and peptides localize at domain boundaries and act as line active agents to modulate membrane shape.

## AUTHOR INFORMATION

### Corresponding Author

*Tel: 713-500-7538. E-mail: Alemayehu.G.Abebe@uth.tmc.edu.

### Notes

The authors declare no competing financial interest.

## ACKNOWLEDGMENTS

This work is partially support by the National Institutes of Health Institute of General Medicine (grant number:

RO1GM100078). Z.L. is supported by the Innovation for Cancer Prevention Research (ICPR) postdoctoral fellowship from Cancer Prevention and Research Institute of Texas (CPRIT, grant number: RP101503). We thank the Texas Advanced Computing Center (TACC) for computational resources. The content is solely the responsibility of the authors and does not necessarily represent the official views of the funding agencies.

## REFERENCES

(1) Frolov, V. A.; Shnyrova, A. V.; Zimmerberg, J. Lipid polymorphisms and membrane shape. *Cold Spring Harbor Perspect. Biol.* **2011**, *3* (11), a004747.
(2) Sackmann, E. Physical Basis of Self-Organization and Function of Membranes: Physics of Vesicles. In *Structure and Dynamics of Membrane*; Handbook of Biological Physics; Elsevier: New York, 1995; Vol. *1*; pp 213−304.
(3) Baumgart, T.; Hess, S. T.; Webb, W. W. Imaging coexisting fluid domains in biomembrane models coupling curvature and line tension. *Nature* **2003**, *425* (6960), 821−824.
(4) Shnyrova, A. V.; Frolov, V. A.; Zimmerberg, J. Domain-driven morphogenesis of cellular membranes. *Curr. Biol.* **2009**, *19* (17), R772−R780.
(5) Lipowsky, R. Budding of membranes induced by intramembrane domains. *J. Phys. II* **1992**, *2* (10), 1825−1840.
(6) Trabelsi, S.; Zhang, S.; Lee, T. R.; Schwartz, D. K. Linactants: surfactant analogues in two dimensions. *Phys. Rev. Lett.* **2008**, *100* (3), 037802.
(7) Brewster, R.; Pincus, P.; Safran, S. Hybrid lipids as a biological surface-active component. *Biophys. J.* **2009**, *97* (4), 1087−1094.
(8) Palmieri, B.; Yamamoto, T.; Brewster, R. C.; A Safran, S. Line active molecules promote inhomogeneous structures in membranes: Theory, Simulations and Experiments. *Adv. Colloid Interface Sci.* **2014**, *208*, 58−65.
(9) Brewster, R.; Safran, S. A. Line active hybrid lipids determine domain size in phase separation of saturated and unsaturated lipids. *Biophys. J.* **2010**, *98* (6), L21−L23.
(10) Yamamoto, T.; Brewster, R.; Safran, S. Chain ordering of hybrid lipids can stabilize domains in saturated/hybrid/cholesterol lipid membranes. *Europhys. Lett.* **2010**, *91* (2), 28002.
(11) Palmieri, B.; Safran, S. A. Hybrid lipids increase the probability of fluctuating nanodomains in mixed membranes. *Langmuir* **2013**, *29* (17), 5246−5261.
(12) Schäfer, L. V.; Marrink, S. J. Partitioning of lipids at domain boundaries in model membranes. *Biophys. J.* **2010**, *99* (12), L91−L93.
(13) Simons, K.; Ikonen, E. Functional rafts in cell membranes. *Nature* **1997**, *387* (6633), 569−572.
(14) Simons, K.; Sampaio, J. L. Membrane organization and lipid rafts. *Cold Spring Harbor Perspect. Biol.* **2011**, *3* (10), a004697.
(15) Konyakhina, T. M.; Goh, S. L.; Amazon, J.; Heberle, F. A.; Wu, J.; Feigenson, G. W. Control of a nanoscopic-to-macroscopic transition: modulated phases in four-component DSPC/DOPC/POPC/Chol giant unilamellar vesicles. *Biophys. J.* **2011**, *101* (2), L8−L10.
(16) Heberle, F. A.; Doktorova, M.; Goh, S. L.; Standaert, R. F.; Katsaras, J.; Feigenson, G. W. Hybrid and nonhybrid lipids exert common effects on membrane raft size and morphology. *J. Am. Chem. Soc.* **2013**, *135* (40), 14932−14935.
(17) Konyakhina, T. M.; Wu, J.; Mastroianni, J. D.; Heberle, F. A.; Feigenson, G. W. Phase diagram of a 4-component lipid mixture: DSPC/DOPC/POPC/chol. *Biochim. Biophys. Acta, Biomembr.* **2013**, *1828* (9), 2204−2214.
(18) Goh, S. L.; Amazon, J. J.; Feigenson, G. W. Toward a better raft model: Modulated phases in the four-component bilayer, DSPC/DOPC/POPC/CHOL. *Biophys. J.* **2013**, *104* (4), 853−862.
(19) Szekely, O.; Schilt, Y.; Steiner, A.; Raviv, U. Regulating the size and stabilization of lipid raft-like domains and using calcium ions as their probe. *Langmuir* **2011**, *27* (24), 14767−14775.
(20) Nicolini, C.; Baranski, J.; Schlummer, S.; Palomo, J.; Lumbierres-Burgues, M.; Kahms, M.; Kuhlmann, J.; Sanchez, S.; Gratton, E.; Waldmann, H. Visualizing association of N-Ras in lipid microdomains: influence of domain structure and interfacial adsorption. *J. Am. Chem. Soc.* **2006**, *128* (1), 192−201.
(21) Weise, K.; Triola, G.; Brunsveld, L.; Waldmann, H.; Winter, R. Influence of the lipidation motif on the partitioning and association of N-Ras in model membrane subdomains. *J. Am. Chem. Soc.* **2009**, *131* (4), 1557−1564.
(22) Janosi, L.; Li, Z.; Hancock, J. F.; Gorfe, A. A. Organization, dynamics, and segregation of Ras nanoclusters in membrane domains. *Proc. Natl. Acad. Sci. U. S. A.* **2012**, *109* (21), 8097−8102.
(23) Li, Z.; Janosi, L.; Gorfe, A. A. Formation and domain partitioning of H-ras peptide nanoclusters: effects of peptide concentration and lipid composition. *J. Am. Chem. Soc.* **2012**, *134* (41), 17278−17285.
(24) Li, Z.; Gorfe, A. A. Deformation of a two-domain lipid bilayer due to asymmetric insertion of lipid-modified Ras peptides. *Soft Matter* **2013**, *9* (47), 11249−11256.
(25) Li, H.; Gorfe, A. A. Aggregation of lipid-anchored full-length H-Ras in lipid bilayers: Simulations with the MARTINI force field. *PloS One* **2013**, *8* (7), e71018.
(26) Levental, I.; Lingwood, D.; Grzybek, M.; Coskun, Ü.; Simons, K. Palmitoylation regulates raft affinity for the majority of integral raft proteins. *Proc. Natl. Acad. Sci. U. S. A.* **2010**, *107* (51), 22050−22054.
(27) Uline, M. J.; Longo, G. S.; Schick, M.; Szleifer, I. Calculating partition coefficients of chain anchors in liquid-ordered and liquid-disordered phases. *Biophys. J.* **2010**, *98* (9), 1883−1892.
(28) Hutchison, J. B.; Weis, R. M.; Dinsmore, A. D. Change of line tension in phase-separated vesicles upon protein binding. *Langmuir* **2012**, *28* (11), 5176−5181.
(29) Hoogerbrugge, P.; Koelman, J. Simulating microscopic hydrodynamic phenomena with dissipative particle dynamics. *Europhys. Lett.* **1992**, *19* (3), 155.
(30) Koelman, J.; Hoogerbrugge, P. Dynamic simulations of hard-sphere suspensions under steady shear. *Europhys. Lett.* **1993**, *21* (3), 363.
(31) Groot, R. D.; Warren, P. B. Dissipative particle dynamics: bridging the gap between atomistic and mesoscopic simulation. *J. Chem. Phys.* **1997**, *107* (11), 4423.
(32) Shillcock, J. C.; Lipowsky, R. Equilibrium structure and lateral stress distribution of amphiphilic bilayers from dissipative particle dynamics simulations. *J. Chem. Phys.* **2002**, *117* (10), 5048−5061.
(33) Illya, G.; Lipowsky, R.; Shillcock, J. Two-component membrane material properties and domain formation from dissipative particle dynamics. *J. Chem. Phys.* **2006**, *125* (11), 114710.
(34) Shillcock, J. C.; Lipowsky, R. Tension-induced fusion of bilayer membranes and vesicles. *Nat. Mater.* **2005**, *4* (3), 225−228.
(35) Kranenburg, M.; Venturoli, M.; Smit, B. Phase behavior and induced interdigitation in bilayers studied with dissipative particle dynamics. *J. Phys. Chem. B* **2003**, *107* (41), 11491−11501.
(36) Rodgers, J. M.; Sørensen, J.; de Meyer, F. J.-M.; Schiøtt, B.; Smit, B. Understanding the phase behavior of coarse-grained model lipid bilayers through computational calorimetry. *J. Phys. Chem. B* **2012**, *116* (5), 1551−1569.
(37) Laradji, M.; Kumar, P. S. Dynamics of domain growth in self-assembled fluid vesicles. *Phys. Rev. Lett.* **2004**, *93* (19), 198105.
(38) Lin, C.-M.; Li, C.-S.; Sheng, Y.-J.; Wu, D. T.; Tsao, H.-K. Size-dependent properties of small unilamellar vesicles formed by model lipids. *Langmuir* **2011**, *28* (1), 689−700.
(39) Li, Z.; Dormidontova, E. E. Kinetics of diblock copolymer micellization by dissipative particle dynamics. *Macromolecules* **2010**, *43* (7), 3521−3531.
(40) Marrink, S. J.; Risselada, H. J.; Yefimov, S.; Tieleman, D. P.; de Vries, A. H. The MARTINI force field: coarse grained model for biomolecular simulations. *J. Phys. Chem. B* **2007**, *111* (27), 7812−7824.

(41) Markvoort, A.; Pieterse, K.; Steijaert, M.; Spijker, P.; Hilbers, P. The bilayer-vesicle transition is entropy driven. *J. Phys. Chem. B* **2005**, *109* (47), 22649−22654.
(42) Plimpton, S. Fast parallel algorithms for short-range molecular dynamics. *J. Comput. Phys.* **1995**, *117* (1), 1−19.
(43) Jülicher, F.; Lipowsky, R. Domain-induced budding of vesicles. *Phys. Rev. Lett.* **1993**, *70* (19), 2964.
(44) Hu, J.; Weikl, T.; Lipowsky, R. Vesicles with multiple membrane domains. *Soft Matter* **2011**, *7* (13), 6092−6102.
(45) Baumgart, T.; Das, S.; Webb, W.; Jenkins, J. Membrane elasticity in giant vesicles with fluid phase coexistence. *Biophys. J.* **2005**, *89* (2), 1067−1080.
(46) Goetz, R.; Lipowsky, R. Computer simulations of bilayer membranes: self-assembly and interfacial tension. *J. Chem. Phys.* **1998**, *108* (17), 7397−7409.
(47) Hess, B. Determining the shear viscosity of model liquids from molecular dynamics simulations. *J. Chem. Phys.* **2002**, *116* (1), 209−217.
(48) Goetz, R.; Gompper, G.; Lipowsky, R. Mobility and elasticity of self-assembled membranes. *Phys. Rev. Lett.* **1999**, *82* (1), 221.
(49) Tolpekina, T.; Den Otter, W.; Briels, W. Simulations of stable pores in membranes: system size dependence and line tension. *J. Chem. Phys.* **2004**, *121* (16), 8014−8020.
(50) Helfrich, W. Elastic properties of lipid bilayers: theory and possible experiments. *Z. Naturforsch., C* **1973**, *28* (11), 693.